catalysts

MDPI

Article

Volatile Hydrogen Intermediates of CO_2 Methanation by Inelastic Neutron Scattering

Jasmin Terreni [1], Olga Sambalova [1], Andreas Borgschulte [1,*], Svemir Rudić [2], Stewart F. Parker [2] and Anibal J. Ramirez-Cuesta [3]

[1] Laboratory for Advanced Analytical Technologies, Empa-Swiss Federal Laboratories for Material Science and Technology, Uberlandstrasse 129, 8600 Dübendorf, Switzerland; jasmin.terreni@empa.ch (J.T.); olga.sambalova@empa.ch (O.S.)

[2] ISIS Facility, STFC Rutherford Appleton Laboratory, Chilton, Didcot OX11 0QX, UK; svemir.rudic@stfc.ac.uk (S.R.); stewart.parker@stfc.ac.uk (S.F.P.)

[3] Oak Ridge National Laboratory, Spallation Neutron Source (SNS), Neutron Spectroscopy Division, Oak Ridge, TN 37831-6475, USA; ramirezcueaj@ornl.gov

* Correspondence: Andreas.Borgschulte@empa.ch

Received: 22 March 2020; Accepted: 7 April 2020; Published: 16 April 2020

Abstract: Despite vast research efforts, the detection of volatile intermediates of catalytic reactions remains a challenge: in addition to the compatibility of the technique to the harsh reaction conditions, a molecular understanding is hampered by the difficulty of extracting meaningful information from operando techniques applied on complex materials. Diffusive reflectance infrared Fourier transform spectroscopy (DRIFTS) is a powerful method, but it is restricted by optical selection rules particularly affecting the detection of hydrogen. This gap can be filled by inelastic neutron scattering (INS). However, INS cannot be used on hydrogenated systems at temperatures higher than 20 K. We demonstrate how its use as a post-mortem method gives insights into the crucial intermediates during CO_2 methanation on Ni/alumina-silica catalysts. We detect a variety of H–, O–, and C-based intermediates. A striking outcome is that hydrogen and oxygen are concurrently chemisorbed on the catalysts, a result that needs the combined effort of DRIFTS and INS.

Keywords: operando vibrational spectroscopy; methanation; nickel; DRIFTS; INS; chemisorbed hydrogen

1. Introduction

Heterogeneous catalysts accelerate chemical reactions by selective binding of the reactants and subsequently formed intermediates on the surface. The number and binding strength of adsorbates is crucial for their functioning. Modern catalysts are complex materials, consisting of various material classes (oxides, metals) structured on length scales from nanometers to millimeters. Thus, their characterisation is an art of its own, and a particular challenge is the in situ detection and quantification of chemical species adsorbed on them. A typical example of this difficulty is the standard method diffusive reflectance infrared Fourier transform spectroscopy (DRIFTS) [1–3]. DRIFTS is a true operando spectroscopy, i.e., it is compatible with the particular sample form (usually powder) and sample environment (gas, liquid) at elevated temperatures and pressures. DRIFTS identifies the main reactants, intermediates, and products adsorbed on the surface as well as in the gas phase during CO_2 methanation catalyzed by Ni particles on alumina/silica as a function of temperature (Figure 1). The qualitative changes are easily recognized, e.g., the occurrence of CO adsorbates at around 180 °C, subsequently followed by the appearance of gaseous methane and water, and many details to be discussed later. However, the signals of the adsorbed as well as gaseous molecules depend

on the infrared(IR)-reflectivity of the catalyst [4–6], which is related to peculiar electronic, optical and structural parameters of the sample in addition to the optical selection rules of IR-spectroscopy [7]. Concretely, DRIFTS on 'black' (no-IR reflectivity) catalysts is very challenging [8], as is the detection and quantification of physisorbed [3] and chemisorbed hydrogen [9–11]. Here, the universality of DRIFTS is disadvantageous: basically, every adsorbate generates an IR-signal, but with highly differing signal intensity; i.e., even if hydrogen chemisorbed on Ni generated an IR-signal, it would be covered by the strong CO-signal [10,12]. However, hydrogen and hydrogen-containing species are the most important molecules of a hydrogenation reaction such as methanation. To shed light on these species, we use the hydrogen selective technique of inelastic neutron scattering (INS) spectroscopy. An INS spectrum is the amplitude of motion and neutron incoherent cross section weighted phonon density of states of both bulk and surface [13]. To emphasize the contribution of the adsorbed species, the spectral contribution from the untreated catalyst is subtracted from the spectra obtained post mortem after the reaction. Given the much higher incoherent scattering cross section of hydrogen (80.26 barn) relative to that of carbon (0.001 barn) and oxygen (0.0008 barn) [13], the spectra reflect the hydrogen partial phonon density of states of adsorbed hydrogen and hydrogen containing molecules, which can be directly compared to the DRIFTS spectra. Despite the promising advantages of INS, the method can only be used post mortem, because the measurement temperature is low (around 20 K).

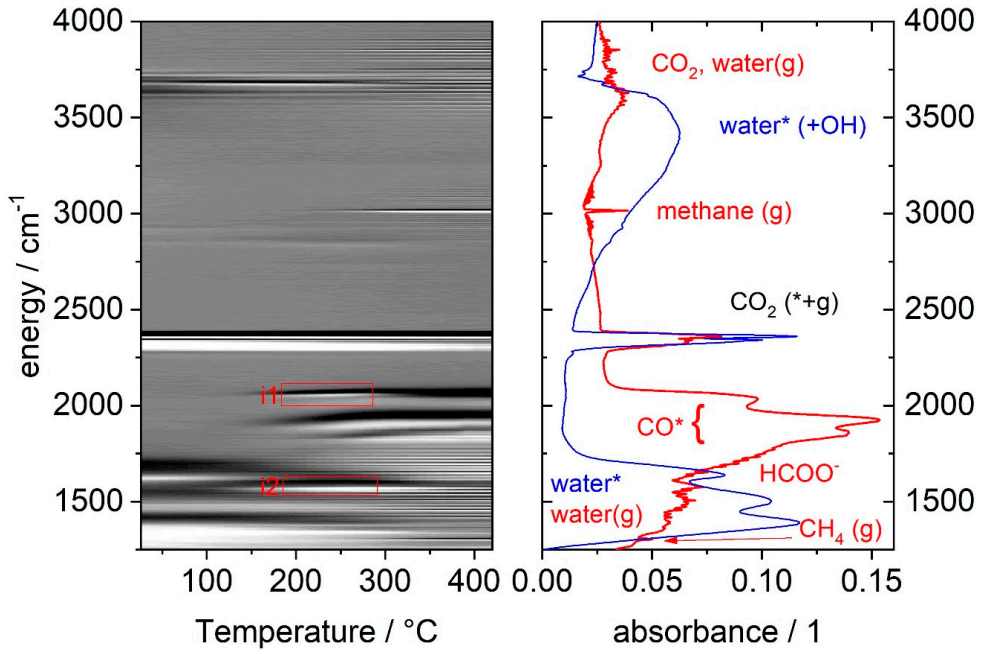

Figure 1. Diffusive reflectance infrared Fourier transform spectroscopy (DRIFTS) spectra of Ni on alumina/silica under methanation conditions between 50 °C and 400 °C. A difficulty of DRIFTS is the varying background with temperature. To emphasize the changes, the spectra were differentiated and plotted as a 2D greyscale image thereby suppressing the broad background. The right panel shows the original starting and final spectra at 50 °C and 400 °C as blue and red curves, respectively. Most obvious adsorbates (*) and gases are assigned, note the change in the intermediates i1 and i2.

In this paper, we demonstrate the use of inelastic neutron scattering by application on the CO_2 methanation reaction catalyzed by a standard Ni-alumina/silica catalyst. As starting point, we discuss DRIFTS measurements, in particular their limitations for the detection of hydrogen species. INS has been applied in systems before, e.g., CO_2 reduction to methanol on Cu/ZnO, [14]. In that study, samples were removed from the reaction cell after the reaction and inserted into the cell for INS measurement. Consequently, detectable adsorbates are limited to strongly bound ones, while volatile intermediates will not survive the experimental procedure. In the paper at hand, we therefore emphasize the transfer strategy for the post-mortem analysis, and estimate the degree of equilibration, i.e., during the transfer

process by the ortho-para conversion of hydrogen [15–17] taking place in parallel. The observations underline that INS facilitates the interpretation of spectra obtained by the true operando method DRIFTS on the very same sample.

2. Results and Discussion

2.1. Experimental boundary conditions of DRIFTS and INS

Both INS and DRIFTS are analysis methods which rely sensitively on the experimental procedure, in particular on the background removal. In a typical DRIFTS experiment, after temperature equilibration of the catalyst in a pure He (H_2) atmosphere a DRIFT spectrum is measured, after which the conditions are changed to H_2 (CO_2 + H_2), while DRIFTS spectra are continuously recorded. The first spectrum is considered to be the background spectrum and is subtracted from all following spectra, hence only showing changes due to evolution of intermediates adsorbed on the surface of the catalyst. There are two main sources of errors of this standard procedure [7] of DRIFTS: changes in the IR-reflectivity of the bulk catalysts may occur and may not be distinguished from surface changes, and the background state of the catalysts is of utmost importance: hardly reversible adsorbates such as water or other oxides will influence the subsequent spectra if they are modified during the course of the reaction. The latter issue is relevant for the INS procedure, too. Firstly, the signal of the empty Inconel 718 sample cell specially designed for flow reactions [18] was measured. Then, 20 g of the sample was added and heated in He-flow to remove adsorbates. The cell was then sealed by closing the valves, removed from the gas handling system, and quenched to 77 K by immersing in liquid nitrogen (Figure 2). Finally, the cell was attached to the INS-sample holder for inelastic neutron scattering measurements at 15 K. For probing the state of the intermediates after the reaction, the sample was exposed to the desired reaction conditions. After equilibration, the cell was closed and quenched to 80 K by immersing the cell in liquid nitrogen. At this temperature, atoms and molecules can be considered to be immobilized, at least within the time needed to further cool the cell down to the measurement temperature of 15 K (2–3 h). The quenching time of around 1 to 2 min is critical: during this time, the reaction proceeds, and thus short-lived intermediates are converted to the subsequent intermediates or even to the final products. The time is given by experimental and technical details such as size and materials properties (heat conductivity) of the cell used.

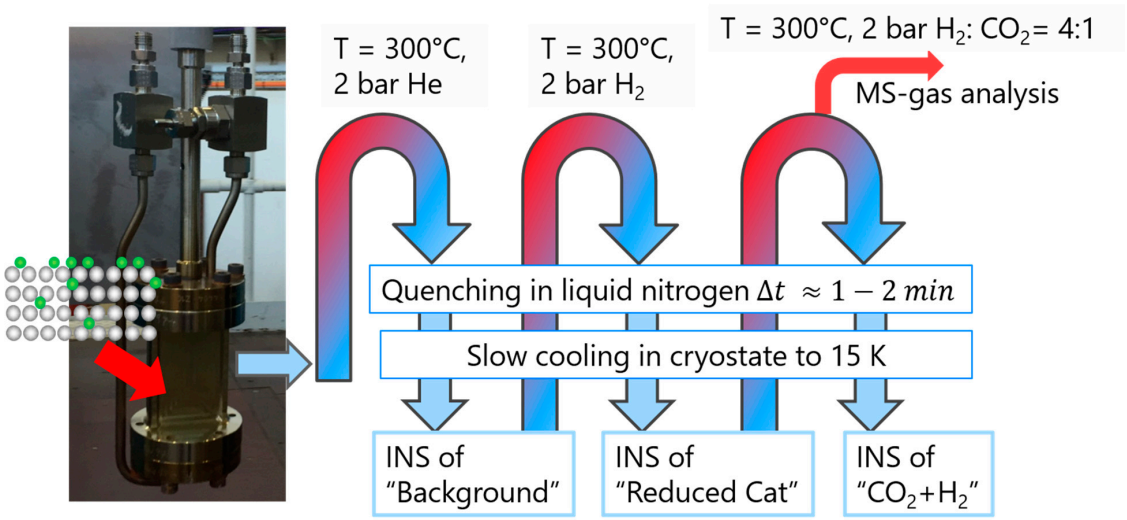

Figure 2. Left: Inconel 718 sample cell specially designed for flow reactions for post-mortem inelastic neutron scattering (INS) [18]. Reduction and methanation takes place at 300 °C in this cell at indicated conditions. The reaction yield is monitored by an attached mass spectrometer. After closing the valves without removing the gases, the cell is quenched to 77 K in liquid nitrogen, and then further cooled down in the cryostat of the neutron beamline (TOSCA).

2.2. Reaction Mechanism of CO_2 Methanation

The methanation reaction (Equation (1)) [19] is one of the oldest catalyzed reactions known to mankind [20,21]. Various d-metals catalyze the reaction with a high degree of conversion and the level of catalyst development is high. The main remaining technical challenges are the control of the heat release in large scale reactors while avoiding hot spots that inactivate the catalyst; and various details associated with poisoning and deactivation of the catalyst [22]. Recently, interest in the reaction increased due to its potential use in a power-to-gas scenario [22]. Here, further development is necessary to push the degree of conversion to minimize energy efficiency losses crucial in renewable energy storage [23]. Furthermore, the reaction is ideal as a model system for studying the fundamental details of catalysis: the reaction mechanism of CO_2 methanation includes adsorption and desorption as well as dissociation and association reactions [24–26]. On pure Ni, the following reaction scheme is commonly assumed (Equations (2)–(7)) [26]:

$$CO_2 + 4H_2 \rightarrow CH_4 + 2H_2O \quad \Delta H = -165\ kJ/mol \tag{1}$$

$$CO_2 + 4H_2 \tag{2}$$

$$\rightarrow CO_2 + 8H^* \quad H_2 - \text{dissociation} \tag{3}$$

$$\rightarrow CO^* + H_2O^* + 6H^* \quad CO - \text{formation} \tag{4}$$

$$\rightarrow C^* + 2H_2O^* + 4H^* \quad C - \text{formation} \tag{5}$$

$$\rightarrow \ CH_n^* + 2H_2O \ ^{(*)\uparrow} \rightarrow +(4-n)H^* \quad C - \text{hydrogenation} \tag{6}$$

$$\rightarrow CH_4 + 2H_2O \tag{7}$$

An asterisk signifies that the molecule is adsorbed; the color code indicates that additional reaction steps are involved, which will be discussed later. A catalyst often consists of metal nano-particles on an oxide support. It is thus not clear where the reaction steps proceed, i.e., where the active sites are located, and where the adsorbates accumulate. If the active site and accumulation site are different, transport phenomena come into play. This can occur between neighboring surface sites via surface diffusion, as, e.g., vividly demonstrated for N_2 dissociation on Ru [27,28], and over relatively large distances between the nanoparticle and its support, also known as the spillover effect [29–31]. With respect to CO_2 methanation on Ni/oxide catalysts, it is commonly accepted that dissociative hydrogen adsorption (Equation (3)) takes place on Ni, while the associative CO_2 adsorption is preferred on the oxide support. Still, the active sites responsible for the subsequent reaction steps are Ni-sites [32]. DFT calculations indicate that similar to the abovementioned case of N_2 dissociation, CO dissociation takes place at these steps. A further conclusion was that although CO and H compete for the same active sites, hydrogen coverage is high at those step sites even at high CO coverages [32]. The characterization of hydrogen on surfaces with the presence of other intermediates is challenging, and was performed only indirectly. Although it is possible to detect chemisorbed hydrogen by infrared spectroscopy, and one study claims to have done so [12], DRIFTS on technical catalysts for chemisorbed hydrogen is practically impossible. In this paper, we present an alternative indication by INS for the co-existence of chemisorbed hydrogen and methanation intermediates.

A technical catalyst contains additional peculiar sites, i.e., the sites at the interface between a Ni-particle and the oxide support [33]. These sites have been postulated as being particularly reactive for CO_2 reduction to CO (Equation (4)) [34], which is assumed to proceed via adsorption to, and reaction with, OH-species:

$$CO_2 \ + OH^* + H^* \rightarrow \ HCO_3^* + H^* \ \rightarrow \ HCOO^* \ + OH^* \tag{8}$$

$$HCOO^* + H^* \rightarrow HCO^* + OH^* \rightarrow CO^* + H^* + OH^* \tag{9}$$

Obviously, the presence and reactivity of OH is crucial. Its occurrence is likely on oxide surfaces, but less so on Ni under reducing conditions, because of water desorbing. On the other hand, hydroxyl groups on oxides are relatively stable, emphasizing the importance of the metal–oxide interface.

$$H^* + OH^* \rightarrow H_2O^{\uparrow} \tag{10}$$

The second complex reaction step (Equation (5)) is the reduction of CO to CH_x species via the direct formation of OH or via chemisorbed oxygen:

$$CO^* + 2H^* \rightarrow \left\{ \begin{array}{l} C^* + OH^* + H^* \\ CH^* + O^* + H^* \end{array} \right\} \rightarrow CH^* + OH^* \tag{11}$$

These details of the mechanism depend sensitively on the interaction of oxygen and hydroxyl with the metal, which are experimentally accessible by the determination of the chemical state of the catalyst, e.g., by operando X-ray absorption fine structure spectroscopy (XAFS) [35] and near-ambient pressure X-ray photoelectron spectroscopy (NAP-XPS) [36–38]) and from theoretical evaluations which are beyond the scope of the present work. However, irrespective of the reaction path, the reactivity of OH is crucial also for this reaction step (5).

Both reaction steps (4,5) generate water, i.e., these steps are affected by the water partial pressure, which is high at high conversion. It is well known that actively removing water increases the overall conversion yield, which is exploited in sorption enhanced catalysis [39] and membrane reactors [40]. There are indications that the distribution of main and side products (CO [39] and soot production [41]) is influenced by the water partial pressure beyond [23] what is expected from thermodynamics [19]. Each of the individual reactions steps (3 to 6) may be rate-limiting, as the slowest step determines the overall reaction kinetics. If the water partial pressure is increased, the individual reaction steps will not be affected equally, which might eventually result in a new rate-limiting step. Furthermore, the concentration of intermediates being reactants of the subsequent, now the rate-limiting step is higher than the that the previous state; and if these intermediates are side products, their yield will be higher, too.

2.3. Infrared Spectroscopy (DRIFTS)

Essentially all reactants (except H_2), intermediates and products of the methanation reaction have a dipole moment, which is affected by molecular vibrations and is, thus, infrared active. DRIFTS is therefore ideal to follow the course of reaction, in particular its dependence on temperature, as shown in Figure 1. Without further input, the onset of the reaction is readily visible around 250 °C, clearest by the appearance of adsorbed CO (around 2000 cm^{-1}) and gaseous CH_4. In particular, this is shown by the change in the intermediates i1 and i2, which are assigned to CO and carbonate (CO_3^{2-}), respectively. The most relevant of the carbon- and oxygen-based compounds are detected with vibrational energies that are in good agreement with published data (for a summary see Table 1).

Table 1. Main hydrogen-, carbon- and oxygen-based vibrations as detected by DRIFTS and INS, all in cm^{-1}.

Species	DRIFTS, This Work	DRIFTS, Ref	INS, This Work	INS, Ref
H on Ni	760	1880 [12]	940, 1140	920, 1093 [42])
CO_{top} on Ni	2033	2070 [43]	-	-
CO_{bridge} on Ni	1919	1944 [43]	-	-
CO_{hollow} on Ni	1845	1880 [43]	-	-
$Ni(CO)_4$	2045	2045 [44]	-	-
$HCOO^-$	1623	-	-	-
CO_3^{2-} species	1570	[45]	-	-
OH	1600, 3500	3500	1600, 3450, 3650	936, 3450 [13,46]
water	1620, 3650	1595, 3657, 3756 [43]	560, 634, 779, 912,	1600, 2280, 3450 1600, 3450 [13]
C-H	see CH_4	see CH_4	1154 1887, 2950	[14]
CH_4	1306, 3017	1305, 3017 [43]	-	-

However, from a catalysis point of view, the detection of intermediates is of great interest to confirm or refute reaction mechanisms as proposed above. The intermediate i1 is very near to vibrations assigned to adsorbed CO at higher temperatures. As its energy (2045 cm^{-1}) is slightly different from the other CO-based vibrations (Table 1), but occurs at only temperatures far below 300°C, we assign it to $Ni(CO)_4$, in good agreement with the literature [44]. $Ni(CO)_4$ is highly unstable, and thus not present at higher temperatures. It is, however, not clear whether it is a mandatory intermediate, or a side product of CO_2 methanation. There are indications that the volatile $Ni(CO)_4$ accelerates the degradation of Ni catalysts due to its volatility (nickel carbonyl-induced particle sintering [47]), and should thus be avoided (by choosing higher temperatures).

The intermediate i2 at 1570 cm^{-1} is less clear, and we assign it to a carbonate species (compare also the different outcomes of Refs. [43,45]).

A particular problem is the region between 1500 and 2000 cm^{-1}, which can be attributed to CO, adsorbed water, OH, and $HCOO^-$ with high uncertainty only (see Figure 3). Only water (and OH) and $HCOO^-$ have IR-transitions in the critical region between 1500 and 2000 cm^{-1}: adsorbed water has a strong peak around 1595 cm^{-1}, overlapping with the C=O stretching mode of $HCOO^-$, expected at 1623 cm^{-1} [48].

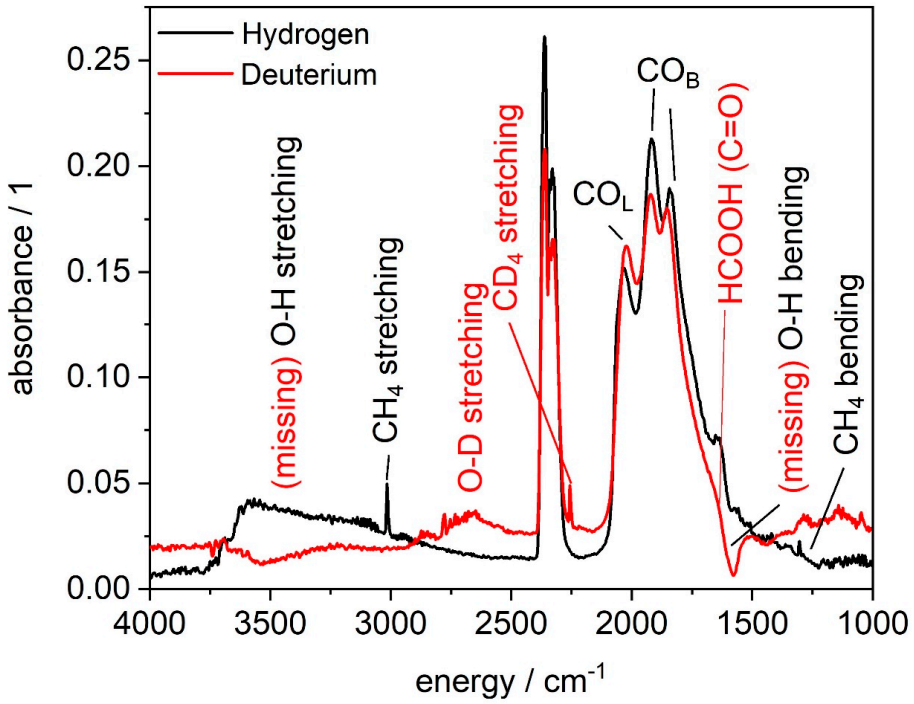

Figure 3. DRIFTS spectra of Ni on alumina/silica under methanation conditions using CO_2 plus hydrogen (black curve) and deuterium (red curve), respectively.

To deconvolute the spectrum, we ran the methanation with deuterium producing the corresponding deuterated intermediates and products. If a compound, which was already present in the DRIFTS background is deuterated, the corresponding spectrum will lack intensity at the positions of the hydrogen-based vibrations. This is readily visible for the ν O–H vibrations of adsorbed water and hydroxyl groups, which show a peak during H-methanation at 3550 cm^{-1} (Figure 3). During D-methanation, a negative peak at 3500 cm^{-1} and a positive peak at 2700 cm^{-1} develop. The small difference between peak and dip is attributed to the fact that the OH groups present during taking the background, i.e., water free conditions, are stable OH (hydroxyl) groups on the oxide support, while water (H_2O) is formed during methanation, which has a slightly lower vibrational energy if adsorbed. CH_4 gas (ν C–H = 3017 cm^{-1}, δ C–H = 1306 cm^{-1}) is not present in the background, and thus a new positive peak arises at 2557 cm^{-1} indicative for the ν C–D stretching vibration of CD_4.

Peaks, which do not shift/disappear are from vibrations without participation of hydrogen, such as CO. In the interesting region between 1500 and 2000 cm^{-1}, a negative peak evolves at 1595 cm^{-1}, while a shoulder at 1625 cm^{-1} remains, which is confirmation for the above assignment of adsorbed water and $HCOO^{-}$. We would like to emphasize that the water peak can be dominating, as it is visible at lower temperatures in Figure 1. The continuous decrease with increasing temperature and the re-developing of the peak with slightly different energy at higher temperature is proof of our assignment, which is in disagreement to that of Zhang et al. [45]. In particular, we interpret the signal from around 1600 cm^{-1} to be mainly OH from water and hydroxyl groups.

However, the most intriguing observation is that despite the need for eight chemisorbed hydrogens per CO_2 to form methane, chemisorbed hydrogen (expected around 1880 cm^{-1} [12]) is not observed. We thus probed the hydrogenated Ni/alumina/silica catalyst by H–D exchange. First, the sample was reduced in hydrogen, and a background spectrum taken. Subsequently, the catalyst was exposed to deuterium gas. Similar to the experiments in Figure 3, we expected to observe negative peaks in the spectrum at H-based vibrations, if they were exchanged by deuterium. Similarly, new positive peaks were expected at shifted energies. Negative and positive peaks were observed, indicative of removed hydrogen and newly formed deuterium-based vibrations, respectively (Figure 4). The principle of H–D exchange is functioning; however, most of the vibrations can be unambiguously assigned to OH and OD. High resolution reflection electron energy loss spectroscopy (HREELS: 1120; 704 [49]; 1035; and 630 cm^{-1} [50]) is in good agreement with the difference spectrum in Figure 4: at around 720 cm^{-1}, a negative peak is observed, possibly due to a Ni-H vibration.

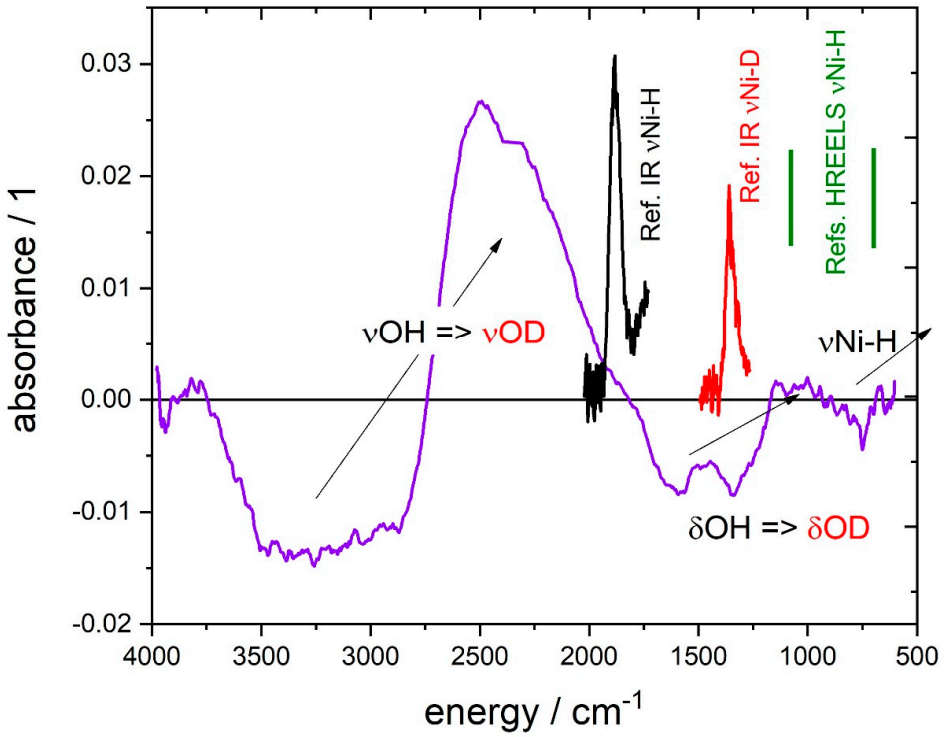

Figure 4. DRIFTS deuterium difference spectrum of Ni on alumina/silica (catalyst exposed to deuterium at room temperature minus background taken after reduction in hydrogen). Reference data on H vibrations on Ni: [12] (IR); high-resolution reflecting electron energy loss spectroscopy (HREELS): 1120 cm^{-1}; 704 cm^{-1} [49]; 1035 cm^{-1}; 630 cm^{-1} [50].

From the literature on IR of Ni-H [12], we expect a negative and positive peak at 1880 and 1360 cm^{-1}, respectively. Unfortunately, these features would overlap with the strong OH vibrations, leaving space for the existence of such vibrations in Ni on alumina/silica. A clear proof requires an additional analytical method. This may be achieved by more advanced IR-techniques such as

2D-infrared spectroscopy, as applied by Palecek et al. on hydrogen chemisorbed on Pt [10]. However, such techniques require very special sample geometries, which is impractical for catalysis research (powder samples etc.).

2.4. Inelastic Neutron Scattering Spectroscopy (INS)

A technique compatible with powder samples and high pressure is INS, which has the severe restriction that it is not an operando technique. However, this post mortem method is very selective to hydrogen, and to a minor extent to Ni, while all other elements with possibly varying surface concentrations are practically invisible to INS. The corresponding incoherent scattering cross sections in barns are $\sigma_{inc}(H) = 80$, $\sigma_{inc}(Ni) = 5.2$, $\sigma_{inc}(O) = 0.0008$, $\sigma_{inc}(C) = 0.001$, $\sigma_{inc}(Al) = 0.0082$, and $\sigma_{inc}(Si) = 0.004$ [13].

Figure 5 shows INS spectra derived by subtracting the spectrum of an empty cell from that of the sample in the cell: Ni on alumina/silica as received, after reduction and after methanation (see also Figure 2). The clearest peaks at 180 and 270 cm^{-1} are ascribed to metallic nickel [51,52], and the low energy structures can be assigned to out-of-plane bend of a hydroxyl [46]. This is expected for a Ni catalyst on an oxide support. Small changes between the spectra indicate the existence of adsorbates after reduction and methanation. Practically identical to the procedure for DRIFTS, these changes are elaborated by plotting the difference spectra between sample states as described in Section 3 and Figure 2. Starting with the reduction process (Figure 6), the general shape of the difference spectrum of the reduced and hydrogen-exposed Ni catalyst matches the reference spectrum of hydrogen exposed Raney nickel catalyst [42] very well, in particular the H-Ni vibrations around 1000 cm^{-1}, and the sharp peak around 100 cm^{-1}, characteristic of para-H_2 physisorbed on Ni. Also, details are resolved: the features between 180 and 270 cm^{-1} can again be ascribed to metallic nickel [51,52], although the number of nickel atoms did not change upon reduction. This means that this intensity must be missing somewhere else. The Ni on alumina/silica catalyst consists of 10–20 nm-sized Ni nanoparticles on an oxide support, which are very reactive and thus easily oxidized. That is, the background spectrum was taken on Ni with an oxide skin, and thus the corresponding peaks at 440 and 580 cm^{-1} [53] occur as negative peaks in the difference spectrum in Figure 6.

Figure 7 shows the difference spectrum of the catalysts exposed to methanation conditions compared to the INS spectrum of water (ice Ih). The overall trend of the catalyst spectrum is very similar to that of water. There is a certain degree of freedom of the absolute intensity. We scaled the water spectrum matching the catalyst spectrum in the spectral range between 100 and 1000 cm^{-1}. There are clear differences at 440 and 580 cm^{-1}, coinciding with a small negative peak at 270 cm^{-1}. This is a very clear indication of the partial reoxidation of the Ni nano-particles during methanation in good agreement with photoemission data [37]. Additionally, we can assign excess intensity around 1000 cm^{-1}, indicative of chemisorbed hydrogen on Ni. This is a surprising result as we also observe NiO. At higher energies, the intensity of the difference spectrum is below that of the water reference. Here, the direct comparison is error prone, because in addition to first order transitions, multi-phonon transitions lead to a relatively broad signal background at higher energies. This intensity is partially removed by background subtraction as conducted for the difference spectra. Still, a comparison of peaks gives indication of the OH (both from water and hydroxyl groups) and CH species (Figure 7).

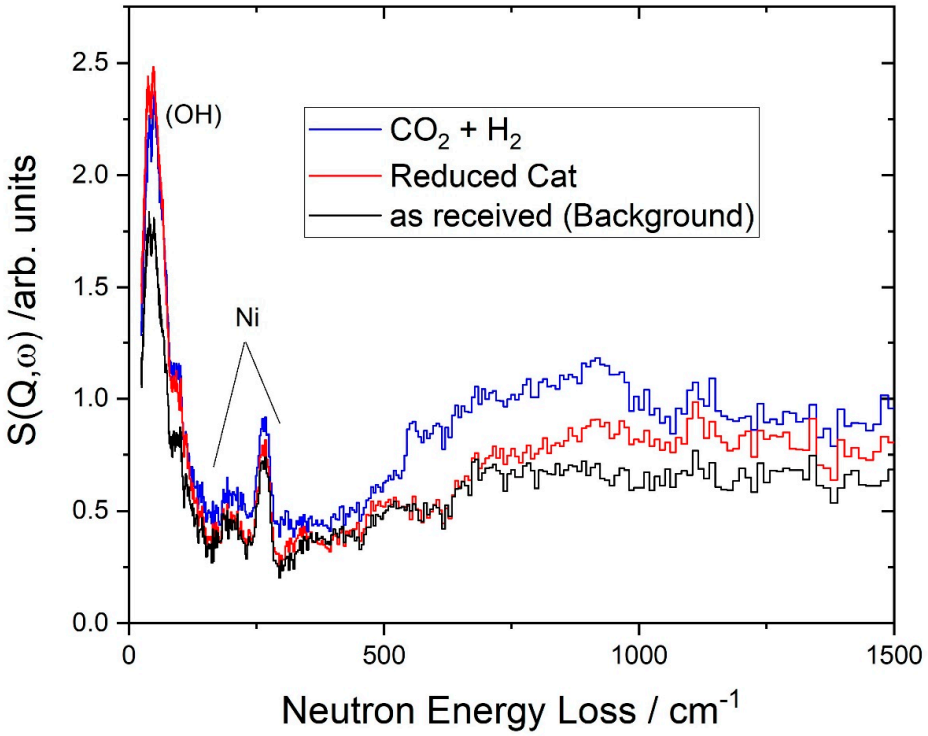

Figure 5. INS spectra as derived by subtracting from the measured spectrum that of the empty sample holder: Ni on alumina/silica as received, after reduction and after methanation (see also Figure 2).

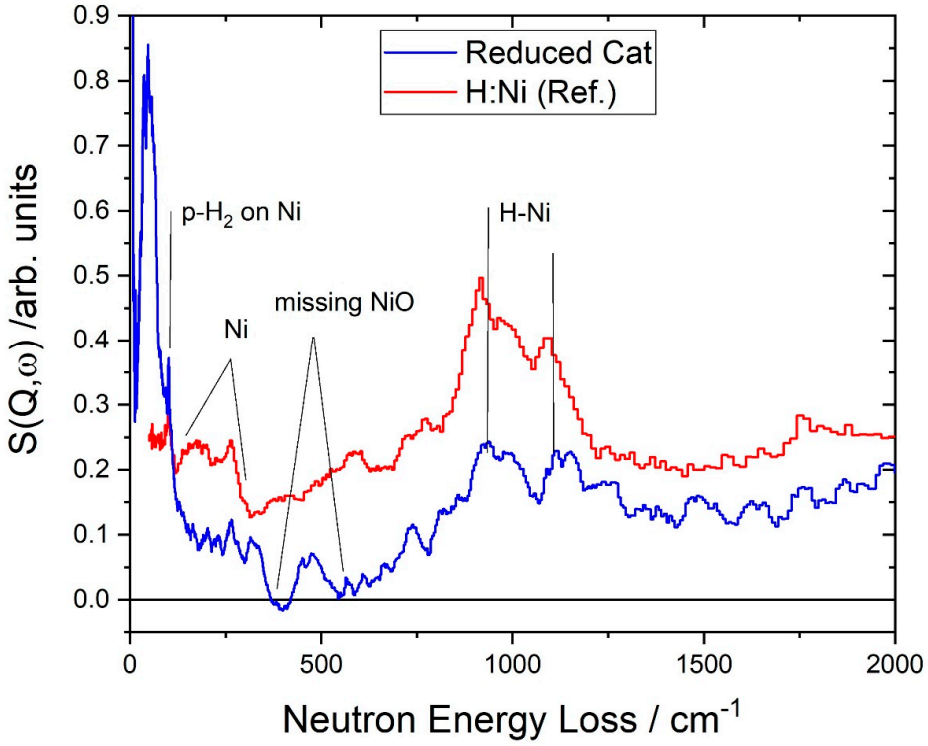

Figure 6. INS difference spectrum of reduced Ni on alumina/silica (blue curve, reduced catalyst minus background, for measurement procedure see Figure 2) compared to a reference spectrum of hydrogen exposed Raney nickel catalyst (red curve, from [43]).

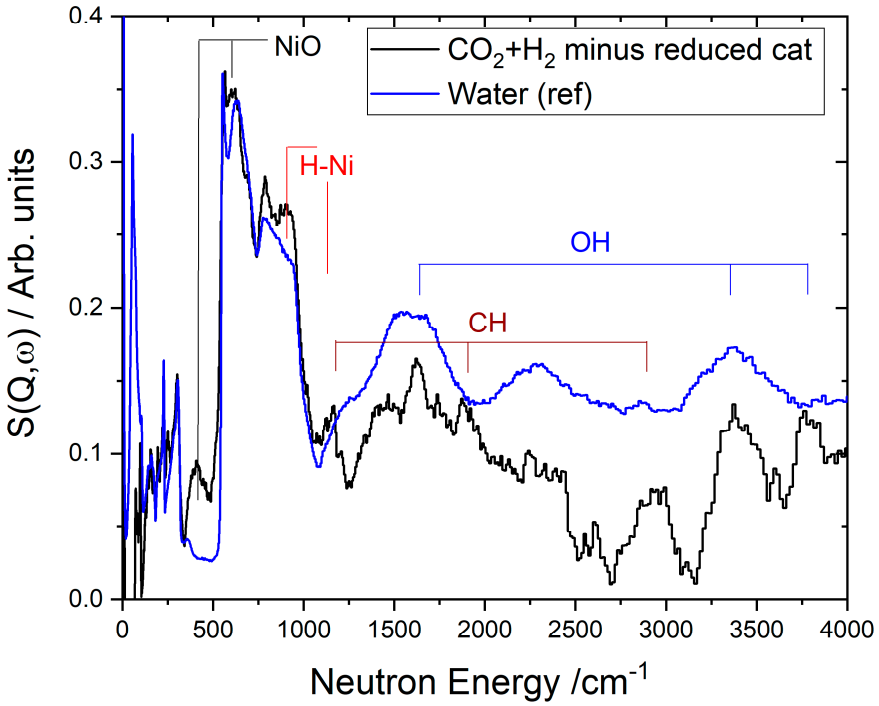

Figure 7. INS difference spectrum of Ni on alumina/silica under methanation conditions (catalyst in CO_2/hydrogen minus reduced catalyst, black curve, for measurement procedure see Figure 2). The blue curve is a INS reference spectrum of water (ice Ih).

2.5. Complementarity of DRIFTS and INS

One goal of spectroscopy in catalysis is to prove or disprove hypotheses on reaction mechanisms; here, on CO_2 methanation, as summarized by Equations (3) to (6). The first step is the identification of the surface adsorbates. Here, DRIFTS is the established method, yielding the most relevant carbon- and oxygen-based compounds for the proposed reaction mechanism. In detail: the detection of CO adsorbed on Ni is strong indication for the reaction step 4. A disadvantage [47] of the presence of CO is the formation of $Ni(CO)_4$, as also evidenced by DRIFTS. DRIFTS delivers arguments for the 'formate pathway' (Equations (8) and (9) by the detection of $HCOO^-$ species. Due to the relatively low sensitivity, DRIFTS gives only hints for the existence of hydrogen chemisorbed to Ni. This demonstrates the need for hydrogen-selective spectroscopy such as INS. Although only a post-mortem method, it gives hard evidence for the presence of chemisorbed hydrogen on the catalyst. An important intermediate, or, alternatively, a reactive species, is OH, which is observed both by DRIFTS as well as INS as hydroxyl in addition to OH vibrations from water. In particular, the facile deuterium hydrogen exchange in OH, even at room temperature, as followed by DRIFTS demonstrates the high reactivity of these species (Figure 4). Less clear results are found to support the formation of C on the surface of Ni (Equation (5)). C–H compounds are detected by DRIFTS and INS, but not in sufficient detail to enlighten the corresponding reaction mechanism. An interesting detail is brought to the fore by INS: the Ni surface consists of NiO and Ni-H, supporting the dissociative pathway from CO to CH without the formation of C via the formation of chemisorbed oxygen (Equation (11)). However, more stringent evidence of this pathway requires the application of a carbon selective operando spectroscopy.

Clearly, the combination of two spectroscopies with different element selectivity can give new insights into the reaction mechanism. It is worth noting that both methods do not have to be operando, if the operando one can be linked to the post-mortem method by preparing well-defined 'quenched-operando' states as demonstrated here.

3. Experimental

The DRIFT spectra were collected using a Vertex 70 infrared spectrometer (Bruker Optics, Zürich, Switzerland) equipped with a DRIFT unit (Praying Mantis, Harrick, Pleasantville, NY, USA) and liquid nitrogen cooled MCT detector. The commercial Harrick cell (HVC-DRP-3) was attached to a gas manifold system.

Inelastic neutron scattering (INS) spectra were recorded at the TOSCA spectrometer of the ISIS Facility of the Rutherford Appleton Laboratory in Didcot, UK [54,55]. The measurements were carried out in neutron energy loss mode at 15 K. The raw data were corrected to obtain the scattering function S(Q,ω) using standard routines available at ISIS within Mantid software package [56].

Experimental conditions for methanation were 1 and 2 bar for DRIFTS and INS, respectively, a CO_2:H_2 ratio of 1:4 and 300 °C. An exception was Figure 1, where the reactive gas mixture was diluted with Ar (CO_2/4H_2:Ar = 1:4). The attached mass spectrometer showed the expected products CO, H_2O and CH_4.

In all cases, we investigated a commercial Ni-alumina/silica catalyst (Sigma-Aldrich, Buchs Switzerland). Its BET-surface area is 175 gm^{-2}, the Ni is 65 weight%.

4. Conclusions

We demonstrate the combination of DRIFTS, an operando spectroscopy, with INS, a post-mortem method, to shine light on the reaction mechanism of CO_2 methanation on Ni/alumina-silica catalysts. We detect a variety of H–, O–, and C-based intermediates. A striking outcome is that hydrogen and oxygen are concurrently chemisorbed on the catalysts, a result which needs the combined effort of DRIFTS and INS.

Author Contributions: J.T., O.S. and A.B. performed the measurements, analysed the results, wrote and revised the paper. S.R. and S.F.P. performed the measurements, analysed and interpreted the INS data, A.J.R.-C. interpreted the INS data. All authors have read and agreed to the published version of the manuscript.

Funding: This research was funded by UZH-UFSP program LightChEC. Swiss National Science Foundation (grant number 172662 and 153928).

Acknowledgments: This work was partly supported by the UZH-UFSP program LightChEC. We also ac-knowledge the financial support from the Swiss National Science Foundation (grant numbers 172662 and 153928). The STFC Rutherford Appleton Laboratory is thanked for access to neutron beam facilities.

Conflicts of Interest: There are no conflicts to declare.

References

1. Hamadeh, I.; King, D.; Griffiths, P. Heatable-evacuable cell and optical system for diffuse reflectance FT-IR spectrometry of adsorbed species. *J. Catal.* **1984**, *88*, 264–272. [CrossRef]
2. Ueckert, T.; Lamber, R.; Jaeger, N.I.; Schubert, U. Strong metal support interactions in a Ni/SiO_2 catalyst prepared via sol-gel synthesis. *Appl. Cat. A* **1997**, *155*, 75–85. [CrossRef]
3. Lamberti, C.; Zecchina, A.; Groppo, E.; Bordiga, S. Probing the surface of heterogeneous catalysts by in-situ IR spectroscopy. *Chem. Soc. Rev.* **2010**, *39*, 4951–5001. [CrossRef] [PubMed]
4. Kubelka, P.; Munk, F.Z. Ein Beitrag Zur Optik der Farbanstriche. *Tech. Phys.* **1931**, *12*, 593–601.
5. Kubelka, P. New Contributions to the Optics of Intensely Light-Scattering Materials. Part I. *J. Opt. Soc. Am.* **1948**, *38*, 448–457. [CrossRef] [PubMed]
6. Little, L.H. *Infrared Spectra of Adsorbed Species*; Academic Press: New York, NY, USA, 1966; pp. 1933–1941.
7. Armaroli, T.; Bécue, T.; Gautier, S. Diffuse Reflection Infrared Spectroscopy (Drifts): Application to the in situ Analysis of Catalysts. *Oil Gas Sci. Technol.-Rev. IFP* **2004**, *59*, 215–237. [CrossRef]
8. Venter, J.J.; Vannice, M.A. Applicability of "drifts" for the characterization of carbon-supported metal catalysts and carbon surfaces. *Carbon* **1988**, *26*, 889–902. [CrossRef]
9. Primet, M.; Basset, J.; Mathieu, M.; Prettre, M. Infrared investigation of hydrogen adsorption on alumina-supported platinum. *J. Catal.* **1973**, *28*, 368–375. [CrossRef]

10. Palecek, D.; Tek, G.; Lan, J.; Iannuzzi, M.; Hamm, P. Characterization of the Platinum-Hydrogen Bond by Surface-Sensitive Time-Resolved Infrared Spectroscopy. *J. Phys. Chem. Lett.* **2018**, *9*, 1254–1259. [CrossRef]
11. Parker, S.F.; Mukhopadhyay, S.; Jiménez-Ruiz, M.; Albers, P.W. Adsorbed States of Hydrogen on Platinum: A New Perspective. *Chem. Eur. J.* **2019**, *25*, 6496–6499. [CrossRef]
12. Nakata, T. Infrared absorption of hydrogen and deuterium chemisorbed on nickel. *J. Chem. Phys.* **1976**, *65*, 487–488. [CrossRef]
13. Mitchell, P.C.H.; Parker, S.F.; Ramirez-Cuesta, A.J.; Tomkinson, J. *Vibrational Spectroscopy with Neutrons with Applications in Chemistry, Biology, Materials Science and Catalysis*; World Scientific Publishing: Singapore, 2005.
14. Kandemir, T.; Friedrich, M.; Parker, S.F.; Studt, F.; Lennon, D.; Schlogl, R.; Behrens, M. Different routes to methanol: Inelastic neutron spectroscopy of adsorbates on supported copper catalysts. *Phys. Chem. Chem. Phys.* **2016**, *18*, 17253–17258. [CrossRef] [PubMed]
15. Alcorn, W.; Sherwood, T. Conversion of parahydrogen to orthohydrogen using nickel/alumina catalysts. *J. Catal.* **1966**, *6*, 288–307. [CrossRef]
16. Matsumoto, M.; Espenson, J.H. Kinetics of the Interconversion of Parahydrogen and Orthohydrogen Catalyzed by Paramagnetic Complex Ions. *J. Am. Chem. Soc.* **2005**, *127*, 11447–11453. [CrossRef] [PubMed]
17. Donaubauer, P.J.; Cardella, U.; Decker, L.; Klein, H. Kinetics and Heat Exchanger Design for Catalytic Ortho-Para Hydrogen Conversion during Liquefaction. *Chem. Eng. Technol.* **2019**, *42*, 669–679. [CrossRef]
18. Warringham, R.; Bellaire, D.; Parker, S.F.; Taylor, J.; Ewings, R.A.; Goodway, C.M.; Kibble, M.; Wakefield, S.R.; Jura, M.; Dudman, M.P.; et al. Sample environment issues relevant to the acquisition of inelastic neutron scattering measurements of heterogeneous catalyst samples. *J. Phys. Conf. Ser.* **2014**, *554*, 012005. [CrossRef]
19. Gao, J.; Wang, Y.; Ping, Y.; Hu, D.; Xu, G.; Gu, F.; Su, F. A thermodynamic analysis of methanation reactions carbon oxides for the production of synthetic natural gas. *RSC Adv.* **2012**, *2*, 2358–2368. [CrossRef]
20. Sabatier, P. Chapter: The Method of Direct Hydrogenation by Catalysis, Nobel lecture 1912. In *Nobel Lectures Chemistry 1901–1921*; Elsevier Publishing Company: Amsterdam, The Netherlands, 1966.
21. Miao, B.; Ma, S.S.K.; Wang, X.; Su, H.; Chan, S.H. Catalysis mechanism of CO_2 and CO methanation. *Catal. Sci. Technol.* **2016**, *6*, 4048–4058. [CrossRef]
22. Rönsch, S.; Schneider, J.; Matthischke, S.; Schlüter, M.; Götz, M.; Lefebvre, J.; Prabhakaran, P.; Bajohr, S. Review on methanation – From fundamentals to current projects. *Fuel* **2016**, *166*, 276–296. [CrossRef]
23. Borgschulte, A.; Callini, E.; Stadie, N.; Arroyo, Y.; Rossell, M.D.; Erni, R.; Geerlings, H.; Züttel, A.; Ferri, D. Manipulating the reaction path of the CO_2 hydrogenation reaction in molecular sieves. *Catal. Sci. Technol.* **2015**, *5*, 4613–4621. [CrossRef]
24. van Herwijnen, T.; van Doesburg, H.; de Jong, W.A. Kinetics of the methanation of CO and CO_2 on a nickel catalyst. *J. Catal.* **1973**, *28*, 391–402. [CrossRef]
25. Fujita, S.I.; Nakamura, M.; Doi, T.; Takezawa, N. Mechanism of methanation of carbon dioxide and carbon monoxide over nickel/alumina catalysts. *Appl. Catal. A* **1993**, *104*, 87–100. [CrossRef]
26. Darensbourg, D.J.; Bauch, C.G.; Ovalles, C. Mechanistic aspects of catalytic carbon dioxide methanation. *Rev. Inorg. Chem.* **1985**, *7*, 315–339. [CrossRef]
27. Nørskov, J.K.; Bligaard, T.; Hvolbæk, B.; Abild-Pedersen, F.; Chorkendorff, I.; Christensen, C.H. The nature of the active site in heterogeneous metal catalysis. *Chem. Soc. Rev.* **2008**, *37*, 2163–2171. [CrossRef] [PubMed]
28. Zambelli, T.; Trost, J.; Wintterlin, J.; Ertl, G. Diffusion and Atomic Hopping of N Atoms on Ru(0001) Studied by Scanning Tunneling Microscopy. *Phys. Rev. Lett.* **1996**, *76*, 795–798. [CrossRef] [PubMed]
29. Conner, W.C.J.; Falconer, J.L. Spillover in Heterogeneous Catalysis. *Chem. Rev.* **1995**, *95*, 759–788. [CrossRef]
30. Prins, R. Hydrogen Spillover. *Facts and FictionChem. Rev.* **2012**, *112*, 2714–2738.
31. Karim, W.; Spreafico, C.; Kleibert, A.; Gobrecht, J.; VandeVondele, J.; Ekinci, Y.; van Bokhoven, J.A. Catalyst support effects on hydrogen spillover. *Nature* **2017**, *541*, 68–71. [CrossRef]
32. Andersson, M.; Abild-Pedersen, F.; Remediakis, I.; Bligaard, T.; Jones, G.; Engbæk, J.; Lytken, O.; Horch, S.; Nielsen, J.; Sehested, J.; et al. Structure sensitivity of the methanation reaction: H_2-induced CO dissociation on nickel surfaces. *J. Catal.* **2008**, *255*, 6–19. [CrossRef]
33. Martin, N.M.; Hemmingsson, F.; Schaefer, A.; Ek, M.; Merte, L.R.; Hejral, U.; Gustafson, J.; Skoglundh, M.; Dippel, A.-C.; Gutowski, O.; et al. Structure-function relationship for CO_2 methanation over ceria spported Rh and Ni catalysts under atmospheric pressure conditions. *Catal. Sci. Technol.* **2019**, *9*, 1644–1653. [CrossRef]

34. Kattel, S.; Liu, P.; Chen, J.G. Tuning Selectivity of CO_2 Hydrogenation Reactions at the Metal/Oxide Interface. *J. Am. Chem. Soc.* **2017**, *139*, 9739–9754. [CrossRef] [PubMed]
35. Mutz, B.; Carvalho, H.W.P.; Mangold, S.; Kleist, W.; Grunwaldt, J.-D. Methanation of CO_2: Structural response of a Ni-based catalyst under fluctuating reaction conditions unraveled by operando spectroscopy. *J. Catal.* **2015**, *327*, 48–53. [CrossRef]
36. Czekaj, I.; Loviat, F.; Raimondi, F.; Wambach, J.; Biollaz, S.; Wokaun, A. Characterization of surface processes at the Ni-based catalyst during the methanation of biomass-derived synthesis gas: X-ray photoelectron spectroscopy (XPS). *Appl. Catal. A* **2007**, *329*, 68–78. [CrossRef]
37. Roiaz, M.; Monachino, E.; Dri, C.; Greiner, M.; Knop-Gericke, A.; Schl¨ogl, R.; Comelli, G.; Vesselli, E. Reverse Water-Gas Shift or Sabatier Methanation on Ni(110)? Stable Surface Species at Near-Ambient Pressure. *J. Am. Chem. Soc.* **2016**, *138*, 4146–4154. [CrossRef]
38. Heine, C.; Lechner, B.A.J.; Bluhm, H.; Salmeron, M. Recycling of CO2: Probing the Chemical State of the Ni(111) Surface during the Methanation Reaction with Ambient-Pressure X-Ray Photoelectron Spectroscopy. *J. Am. Chem. Soc.* **2016**, *138*, 13246–13252. [CrossRef]
39. Borgschulte, A.; Gallandat, N.; Probst, B.; Suter, R.; Callini, E.; Ferri, D.; Arroyo, Y.; Erni, R.; Geerlings, H.; Züttel, A. Sorption enhanced CO_2 methanation. *Phys. Chem. Chem. Phys.* **2013**, *15*, 9620–9625. [CrossRef]
40. Ohya, H.; Fun, J.; Kawamura, I.; Itoh, K.; Ohashi, H.; Aihara, M.; Tanisho, S.; Negishi, Y. Methanation of carbon dioxide by using membrane reactor integrated with water vapor permselective membrane and its analysis. *J. Membr. Sci.* **1997**, *131*, 237–247. [CrossRef]
41. Delmelle, R.; Terreni, J.; Remhof, A.; Heel, A.; Proost, J.; Borgschulte, A. Evolution of Water Diffusion in a Sorption-Enhanced Methanation Catalyst. *Catalysts* **2018**, *8*, 341. [CrossRef]
42. Parker, S.F.; Bowron, D.T.; Imberti, S.; Soper, A.K.; Refson, K.; Lox, E.S.; Lopez, M.; Albers, P. Structure determination of adsorbed hydrogen on a real catalyst. *Chem. Commun.* **2010**, *46*, 2959–2961. [CrossRef]
43. Zarfl, J.; Ferri, D.; Schildhauer, T.J.; Wambach, J.; Wokaun, A. DRIFTS study of a commercial Ni/γ-Al_2O_3 CO methanation catalyst. *Appl. Catal. A Gen.* **2015**, *495*, 104–114. [CrossRef]
44. Mihaylov, M.; Hadjiivanov, K.; Knozinger, H. Formation of $Ni(CO)_4$ during the Interaction between CO and Silica-Supported Nickel Catalysts: An FTIR Spectroscopic Study. *Catal. Lett.* **2001**, *76*, 59–63. [CrossRef]
45. Zhang, Z.; Tian, Y.; Zhang, L.; Hu, S.; Xiang, J.; Wang, Y.; Xu, L.; Liu, Q.; Zhang, S.; Hu, X. Impacts of nickel loading on properties, catalytic behaviors of Ni/γ-Al_2O_3 catalysts and the reaction intermediates formed in methanation of CO_2. *Int. J. Hydrog. Energy* **2019**, *44*, 9291–9306. [CrossRef]
46. Parker, S.F. The role of hydroxylgroups in low temperature carbon monoxide oxidation. *Chem. Commun.* **2011**, *47*, 1988–1990. [CrossRef] [PubMed]
47. Barrientos, J.; Gonzalez, N.; Lualdi, M.; Boutonnet, S.; Jaras, M. The effect of catalyst pellet size on nickel carbonyl-induced particle sintering under low temperature CO methanation. *Appl. Catal. A* **2016**, *514*, 91–102. [CrossRef]
48. Forney, D.; Jacox, M.E.; Thompson, W.E. Infrared spectra of trans-HOCO, $HCOO^+$, and HCO_2^- trapped in solid neon. *J. Chem. Phys.* **2003**, *119*, 10814–10823. [CrossRef]
49. Ho, W.; DiNardo, N.J.; Plummer, E.W. Angle-resolved and variable impact energy electron vibrational excitation spectroscopy of molecules adsorbed on surfaces. *J. Vac. Sci. Technol.* **1980**, *17*, 134–140. [CrossRef]
50. Voigtlander, B.; Lehwald, S.; Ibach, H. Hydrogen adsorption and the adsorbate-induced Ni(110) reconstruction-an EELS study. *Surf. Sci.* **1989**, *208*, 113–135. [CrossRef]
51. Birgeneau, R.J.; Cordes, J.; Dolling, G.; Woods, A.D.B. Normal Modes of Vibration in Nickel. *Phys. Rev.* **1964**, *136*, A1359–A1365. [CrossRef]
52. Kresch, M.; Delaire, O.; Stevens, R.; Lin, J.Y.Y.; Fultz, B. Neutron scattering measurements of phonons in nickel at elevated temperatures. *Phys. Rev. B* **2007**, *75*, 104301. [CrossRef]
53. Dietz, R.E.; Parisot, G.I.; Meixner, A.E. Infrared Absorption and Raman Scattering by Two-Magnon Processes in NiO. *Phys. Rev. B* **1971**, *4*, 2302–2310. [CrossRef]
54. Parker, S.F.; Fernandez-Alonso, F.; Ramirez-Cuesta, A.J.; Tomkinson, J.; Rudic, S.; Pinna, R.S.; Gorini, G.; Castanon, J.F. Recent and future developments at TOSCA at ISIS. *J. Phys. Conf. Ser.* **2014**, *554*, 012003. [CrossRef]

55. Pinna, R.S.; Rudić, S.; Parker, S.F.; Armstrong, J.; Zanetti, M.; Škoro, G.; Waller, S.P.; Zacek, D.; Smith, C.A.; Capstick, M.J.; et al. The neutron guide upgrade of the TOSCA spectrometer. *Nucl. Instrum. Methods Phys. Res. Sect. A Accel. Spectrometers Detect. Assoc. Equip.* **2018**, *896*, 68–74. [CrossRef]
56. Arnold, O.; Bilheux, J.C.; Borreguero, J.M.; Buts, A.; Campbell, S.I.; Chapon, L.; Doucet, M.; Draper, N.; Leal, R.F.; Gigg, M.A. Mantid—Data analysis and visualization package for neutron scattering and μ SR experiments. *Nucl. Instrum. Methods Phys. Res. Sect. A Accel. Spectrometers Detect. Assoc. Equip.* **2014**, *764*, 156–166. [CrossRef]